Applied Catalysis B: Environmental 140–141 (2013) 32–41

Contents lists available at SciVerse ScienceDirect

Applied Catalysis B: Environmental

journal homepage: www.elsevier.com/locate/apcatb

Electrochemical photocatalytic degradation of dye solution with a TiO_2-coated stainless steel electrode prepared by electrophoretic deposition

Wei-Chieh Lin [a], Chien-Hung Chen [a], Han-Yu Tang [a], Yu-Cheng Hsiao [c], Jill Ruhsing Pan [b], Chi-Chang Hu [c,*], Chihpin Huang [a,*]

[a] Institute of Environmental Engineering, National Chiao Tung University, 1001 University Road, Hsin-Chu, 30010, Taiwan
[b] Department of Biological Science and Technology, National Chiao Tung University, 75 Po-ai Street, Hsin-Chu, 30068, Taiwan
[c] Department of Chemical Engineering, National Tsing Hua University, 101, Section 2, Kuang-Fu Road, Hsin-Chu, 30013, Taiwan

ARTICLE INFO

Article history:
Received 21 November 2012
Received in revised form 1 March 2013
Accepted 20 March 2013
Available online 1 April 2013

Keywords:
Photocatalytic degradation
Electrochemical Fenton reaction
Dye
Electrophoretic deposition
Titanium dioxide

ABSTRACT

This study demonstrates a new model for the treatment of azo dye wastewater by means of a heterogeneous photocatalytic degradation coupled with the homogeneous electrochemical Fenton reaction, and is called electrochemical photocatalytic (ECPC) degradation. Titanium dioxide-coated stainless steel (P25-TiO_2/SS) mesh was employed as a photo-anode, covered with a uniform layer of P_{25}-TiO_2 using electrophoretic deposition (EPD) in a 2-propanol suspension with 10^{-4} M $Zn(NO_3)_2$, at a deposition time of 1 min. After annealing in air at 350 °C for 1 h, a crack-free, porous P25-TiO_2 layer of ca. 2.14 μm was obtained. Potential bias was used to enhance the photocatalytic degradation of P25-TiO_2/SS towards the target pollutant, azo dye orange G, in an undivided cell under ultraviolet light irradiation. Heterogeneous photocatalytic degradation and a homogeneous electro-Fenton reaction occurred in the system simultaneously when H_2O_2 and Fe^{2+} were electrochemically generated on the graphite cathode and photo-anode, respectively, under a suitable potential bias, enhancing the de-colorization and removal of total organic carbon.

1. Introduction

In the past few decades, bio-degradation [1], electrocoagulation [2], electrochemical oxidation [3,4], and other similar methods have been commonly proposed in wastewater treatment systems. However, serious constraints were discovered in using these technologies, such as long reaction time for bio-degradation and an ion removal issue for electrocoagulation. Moreover, certain pollutants, such as those in dye wastewater, cannot be effectively removed or decomposed by the above methods. Consequently, advanced oxidation processes (AOPs) such as photocatalytic degradation [5] and Fenton oxidation [6] were developed to achieve better removal efficiencies compared with traditional processes. Fenton oxidation, for example, employs hydroxyl radicals ($OH^•$) and other strong oxidants to remove organics through direct and indirect processes.

Fenton reagent is a strong oxidant for organic degradation and de-colorization [7,8] because of the redox reaction between the Fe^{3+}/Fe^{2+}-couple and H_2O_2 that generates highly reactive hydroxyl and peroxide radicals ($OH^•$ and $OOH^•$). Mixing H_2O_2 and Fe^{2+} is the simplest method for obtaining Fenton reagent for organic degradation. Some in situ methods involve electrochemical steps. The electro-Fenton process involves the following reactions: electrochemical dissolution of Fe^{2+} from an iron anode [9], electrochemical reduction of Fe^{3+} to produce Fe^{2+} [10] for continuous reaction with H_2O, or the electrochemical reduction of O_2 to produce H_2O_2 [2,11] for reacting with the Fe^{3+}/Fe^{2+} couple [10]. Since the continuous regeneration of Fe^{2+} at the cathode has been found to reduce sludge production [12], the simultaneous electrochemical reduction of Fe^{3+} to Fe^{2+} and the electrochemical generation of H_2O_2 at the cathode fed with O_2/air was proposed to avoid the repetitive addition of reagents, and to achieve the high removal efficiency of organic pollutants [13].

For photocatalytic degradation, titanium dioxide, a typical n-type semiconductor, has been demonstrated to be an effective photocatalyst in AOPs because of its excellent chemical stability, high photo efficiency, non-toxicity, and reasonable cost [13]. Since the band gap of P25-TiO_2 is ca. 3.0–3.2 eV [14], electrons and holes need to be photo-excited to the conduction and valence bands, respectively, by UV-light illumination. The photo-excited electrons may flow to the cathode to drive certain reduction processes (e.g.,

* Corresponding authors. Tel.: +886 35712121x55507; fax: +886 35725958.
E-mail addresses: cchu@che.nthu.edu.tw (C.-C. Hu), cphuang@mail.nctu.edu.tw (C. Huang).

0926-3373/$ – see front matter © 2013 Elsevier B.V. All rights reserved.
http://dx.doi.org/10.1016/j.apcatb.2013.03.032

H_2O_2 generation and H_2 evolution), while the holes may drive direct or indirect [15,16] oxidation processes. Unfortunately, the efficiency of photocatalytic reactions on TiO_2 is relatively low (<5%) [17] as a result of the high electron–hole recombining rate. Hence, the use of suitable electron/hole scavengers, the presence of surface defect states, or applying positively biased potentials on the photo-anode have been widely recommended to circumvent the problem of photo-generated electron–hole recombination [18]. Among the above three strategies, the third method, electro-photocatalytic degradation [19], one of the electro-assisted advanced oxidation processes (EAOPs), generally results in high efficiencies of organic removal.

Based on the above information, it becomes possible to integrate electro-Fenton and electro-photocatalytic degradation processes. This newly developed EAOP, named electrochemical photocatalytic degradation, combines all the advantages of the above two advanced processes, and seems to be a promising method for treating pollutants that are difficult to remove or degrade by commonly applied processes. In this study an electrochemical photocatalytic degradation process was carried out in a cell with a P25-TiO_2-coated SS mesh photo-anode to drive both heterogeneous photocatalytic degradation and Fe^{2+} generation. Further, an electrocatalytic cathode was used to generate H_2O_2 and reduce Fe^{3+} for homogeneous Fenton oxidation. Although the TiO_2 coating can be prepared by various methods, such as dip-coating [20,21], screen printing [22,23], chemical vapor deposition [24,25], anodization [26], electrochemical deposition [27,28], or electrophoretic deposition (EPD) [29], EPD was used to prepare the P25-TiO_2/SS photo-anode for this study, because of its high versatility and cost-effectiveness [30]. Furthermore, the influence of Pt and graphite as cathode materials, for H_2O_2 generation and Fe^{3+} reduction on the removal efficiency of dye orange G were compared. In addition, the effects of the process parameters such as pH value of wastewater, UV illumination, and biased potential on orange G decontamination were also investigated. This newly developed electrochemical photocatalytic degradation process with a P25-TiO_2/SS photo-anode biased at 1.0 V (vs. SCE) under UV illumination and a graphite cathode with air bubbling showed promising performances for orange G mineralization.

2. Experimental

2.1. Materials

Azo acid dye orange G (OG, chemical reagent grade, Sigma–Aldrich) was used as the target pollutant. P25-TiO_2 powder (80% anatase phase and 20% rutile structure; Degussa AG), with an average particle size of 21 nm and a specific area of 50 m^2/g were employed as the electrode material, coated onto a stainless steel mesh (SUS304, 200 mesh). Platinum (2 cm × 5 cm) and graphite (2 cm × 5 cm) sheets (Sigma–Aldrich) were used as the cathode for the electrochemical photocatalytic degradation system, while two platinum (2 cm × 5 cm) sheets were employed as the anode for the EPD process. The inorganic reagents H_2SO_4 (95–97%, 30743-1L, Sigma–Aldrich Co. Ltd.), Na_2SO_4 (3375-01, J.T. Baker) and $Zn(NO_3)_2$ (4344-01, J.T. Baker), as well as the organic reagents ethanol (1311086.1211, Panreac), 2-propanol (33539, Sigma–Aldrich Co. Ltd.), and acetone (actual analysis, 2440-08, Macron) were used without further purification.

2.2. Preparation of P25-TiO_2/SS mesh electrode

The P25-TiO_2/SS mesh electrode was prepared by coating P25-TiO_2 powders onto SS mesh by EPD procedure. To clean up and roughen the surface of the (2 cm × 5 cm) raw SS mesh, it was first washed ultrasonically in 0.98 M H_2SO_4 for 60 min and then in acetone for 40 min, fully rinsed with DI water, and dried using a N_2-airgun before EPD processing.

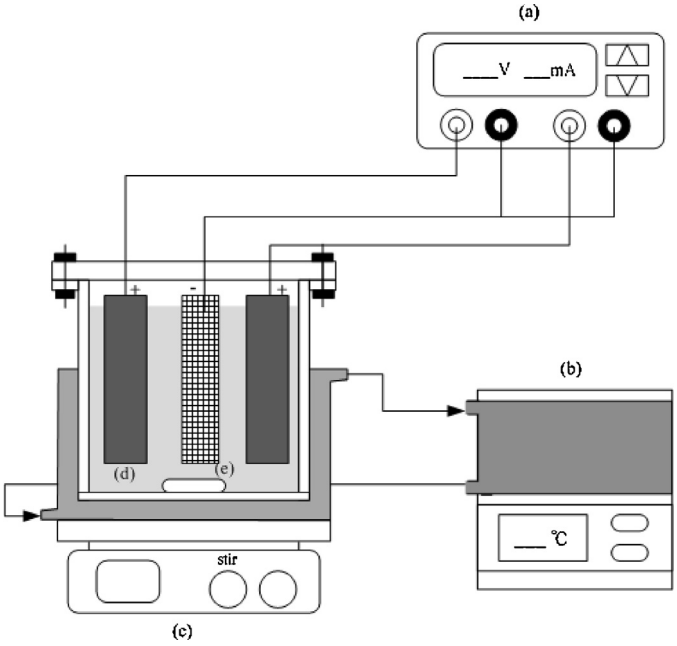

Fig. 1. A schematic diagram of the electrophoretic deposition equipment: (a) the power supply, (b) a water thermostat, (c) magnetic stir, (d) the Pt sheet anode (2 cm × 5 cm), (e) the 304 SS mesh cathode (2 cm × 5 cm).

For the EPD process, the SS mesh was placed vertically at the center of a 250 mL jacket cell, facing two Pt sheets for depositing the P25-TiO_2 film. A schematic diagram of the EPD system is shown in Fig. 1. A 200 mL 2-propanol solution containing 10^{-4} M $Zn(NO_3)_2$ and 3.2 g L^{-1} P25-TiO_2 was used as the deposition solution, in which $Zn(NO_3)_2$ was used to enhance the uniformity and adhesion of P25-TiO2 on the SS substrates as determined in preliminary tests. Electrophoretic deposition was conducted at 4 °C under an applied electric field of 180 V for different EPD periods, and then the P25-TiO_2/SS electrodes, rinsed with DI water, were annealed in air at various temperatures for 60 min. The dye-sensitized solar cell for the photovoltaic test and the TiO_2-coated FTO electrode for the photo-electrochemical study were acquired from the Everlight Chemical Co., Taiwan.

2.3. Electrochemical photo-degradation reactor and experimental procedure

Electrochemical photocatalytic degradation was tested in a batch-scale three-electrode system with P25-TiO_2/SS as the working electrode, Pt or graphite as the counter electrode, and SCE as the reference electrode. A schematic diagram of the electrochemical photochemical reactor system is shown in Fig. 2. The test solution contained 0.01 M Na_2SO_4 and 64.0 mg L^{-1} orange G with pH 3.0 adjusted with 0.5 M H_2SO_4. The photo-electrode (or the graphite electrode) potential was biased at 1.0 V (or −1.0 V). UV light at a wavelength of 365 nm with a power density of 330 μW cm^{-2} (Entela UVGL-25) was provided on the photo-electrode side of the reactor. To generate H_2O_2, O_2 gas was provided for the Pt or graphite electrodes at a flow rate of 50 mL min^{-1}. The pH values of the test solution between 6.0 and 9.0 were adjusted with 0.5 M H_2SO_4 and 1.0 M NaOH.

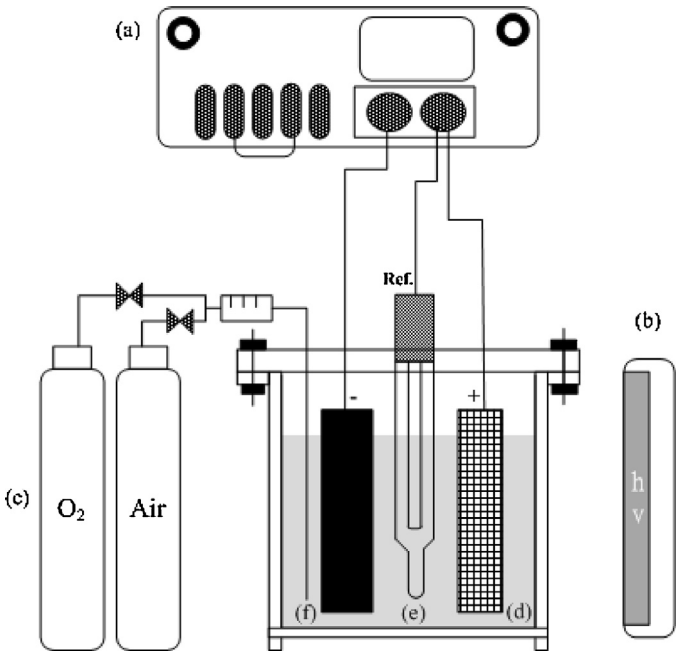

Fig. 2. A schematic diagram of the electrochemical photocatalytic reactor: (a) the potentiostat, (b) the UV lamp (365 nm, 4 W), (c) an O_2 gas flow (50 mL min^{-1}), (d) the P25-TiO_2/SS electrode (2 cm × 5 cm), (e) the saturated calomel reference electrode (SCE); (f) the Pt or graphite counter electrode (2 cm × 5 cm).

2.4. Analytical methods

The surface morphology and thickness of the P25-TiO_2 coatings were checked by scanning electron microscopy (SEM) (Hitachi S-4700I). The XRD patterns of all photo-electrodes were recorded with an X-ray diffractometer (XRPD-WAG, Rigaku TTRAX III, Cu Kα, with an accelerating voltage of 40 V) at a scan rate of 4° min^{-1} (2θ from 20° to 80°). The BET surface area analysis was conducted by Tristar 3000. Linear sweep voltammetry (LSV), cyclic voltammetry (CV), and chronoamperometry were performed using a Potentionstat/Galvanostat (AutoLab). The concentrations of H_2O_2 and Fe^{2+} in the test solution were measured by the N,N-diethyl- p-phenylenediamine (DPD) and tripyridylstriazine (TPTZ) methods, respectively. The UV–vis absorption spectra of the test solution for orange G dye were measured by a Hitachi U3010 Spectrophotometer. The dissolved organic carbon (DOC) concentration was measured by SIEVERS TOC M800.

3. Results and discussion

3.1. Characterization of TiO_2/SS mesh electrodes

Fig. 3 shows the dependence of the mass of P25-TiO_2 deposited onto the SS mesh on the duration of EPD. The mass of P25-TiO_2 increased from 0.36 to 1.81 mg cm^{-2} with the increase of EPD time from 1 to 5 min. The deposition of P25-TiO_2 onto the SS mesh (the negative electrode) was brought about by the positive charge of P25-TiO_2 in the 2-propanol solution containing 0.1 mM $Zn(NO_3)_2$, and the rate of deposition was a function of the bath temperature and the electric voltage applied in the process. Preliminary results indicated that suitable suspension temperature and applied electric field were 4 °C and 180 V, respectively.

The linear relationship between the P25-TiO_2 mass and the EPD time can be described by a model proposed previously [31], where

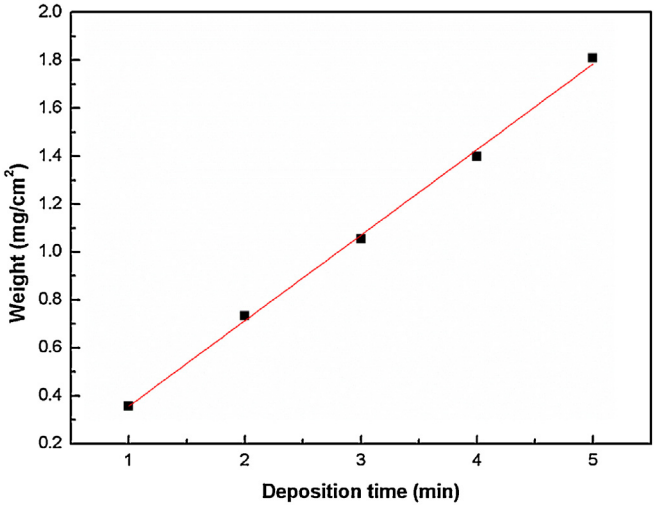

Fig. 3. Dependence of the P25-TiO_2 mass on the EPD time at an applied electric field of 180 V from a 2-propanol solution containing 10^{-4} M $Zn(NO_3)_2$ and 3.2 g L^{-1} P25-TiO_2 at 4 °C.

the rate of mass (m) deposited onto the substrate is an exponential function of the EPD time, and is expressed as:

$$\frac{dm(t)}{dt} = w_0 k \exp(-k't) \quad (1)$$

and

$$k = \frac{A}{V}\frac{\varepsilon\xi}{4\pi\eta}(E - \Delta E) \quad (2)$$

where m is the mass of the solid particle deposited on the electrode, k and k' are kinetic constants, t is the deposition time, A is the geometric area of the electrode, V is the volume of suspension, w_0 is the initial weight of the solid particle in the suspension, ε is the dielectric constant of the liquid, ξ is the zeta potential of the particle in the solvent, η is the viscosity of the liquid, E is the applied DC electric field, and ΔE is the voltage drop across the deposited layer. Furthermore, with a short EPD, Eq. (1) can be simplified as below:

$$m(t) = w_0 kt = w_0 \frac{A}{V}\frac{\varepsilon\xi}{4\pi\eta}(E - \Delta E)t \quad (3)$$

From Eq. (3), the mass of P25-TiO_2 is directly proportional to the EPD time when the EPD time is short. This phenomenon indicates a constant deposition rate during this short EPD time. Based on the excellent linearity between the mass of P25-TiO_2 and the EPD time, the EPD behavior of P25-TiO_2 particles onto the SS mesh could within 5 min be suitably described by the proposed model.

Fig. 4 shows the XRD patterns of the SS substrate with annealing at 450 °C and P25-TiO_2/SS (EPD time = 1 min) without and with annealing from 350 to 650 °C. In comparing all patterns, three features must be mentioned. First, the diffraction peaks corresponding to the SS substrate are also visible on the XRD patterns of P25-TiO_2/SS electrodes, indicating that the thickness of such a P25-TiO_2 film should be thinner than 5 μm. Second, the deposited P25-TiO_2 layers without and with annealing at temperatures ≤550 °C retain a similar crystalline structure to that of the P25-TiO_2 particles. The predominant crystalline phase of P25-TiO_2 is anatase (A-TiO_2), corresponding to the characteristic diffraction peaks centered at 25.4° and 48.1° for facets (1 0 1) and (2 0 0), respectively. These results reveal the thermal stability of P25-TiO_2 at temperatures ≤550 °C. Third, when the annealing temperature is set at 650 °C, the diffraction peak centered at 27.5° becomes visible, corresponding to facet (1 1 0) of the rutile form (R-TiO_2). At the same time, the intensities of the diffraction peaks corresponding to facets (1 0 1) and (2 0 0) in

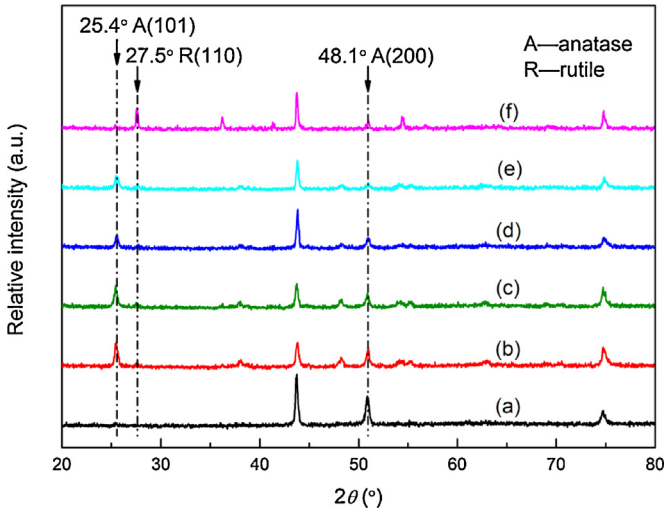

Fig. 4. XRD patterns of (a) a SS mesh annealed at 450 °C, (b) as-prepared P25-TiO_2/SS, and P25-TiO_2/SS annealed at (c) 350, (d) 450, (e) 550, (f) 650 °C.

the anatase phase decrease significantly. These phenomena indicate that annealing at or above 650 °C for 1 h can cause the phase transformation of TiO_2 from the anatase form into the rutile structure. This is consistent with the results reported in the literature [32]. In general, P25-TiO_2 exhibits a higher photocatalytic activity than both pure A- and R-TiO_2 [33]. Thus, to retain the high photocatalytic activity of P25-TiO_2 and to improve the adhesion of the P25-TiO_2 layer on the SS substrate, all TiO_2/SS electrodes for electrochemical photocatalytic degradation were annealed at 350 °C for 1 h.

The surface morphology of P25-TiO_2 films on the SS mesh was examined from SEM images, and typical SEM photographs are shown in Fig. 5. The diameter of SS wire and the pore size of a bare SS mesh are about 70 μm. The surface of SS wires is compact and relatively smooth. After 1 min deposition time, the pore size of P25-TiO_2/SS mesh was reduced to ca. 65 μm and the surface of SS wires had a uniform but rough coating of P25-TiO_2 without visible micro-cracks. However, some micro-cracks were observed in the P25-TiO_2 layer when the EPD time reached 3 min, and the pore size of TiO_2/SS mesh was reduced to ca. 45 μm. Moreover, when the deposition time was set at 5 min, the shape of the SS mesh pores changed from square into circular with a mean pore size of ca. 15 μm. Since the thickness and micro-cracks of P25-TiO_2 films might increase the charge-transfer resistance of photo-excited electrons, the EPD time in this work was fixed at 1 min.

The cross-sectional SEM image of P25-TiO_2/SS with an EDP time of 1 min is shown in Fig. 6a, showing a thickness of 2.14 μm for this EPD P25-TiO_2 layer, with a rough morphology. Moreover, under high magnification (see Fig. 6b), the mean particle size of P25-TiO_2 on the SS substrate was seen to be about 21 nm, which is close to that of the original P25-TiO_2 powders. Based on the above results, the original characteristics of P25-TiO_2 were not changed by the EPD process and annealing at 350 °C for 1 h.

3.2. Effect of cathode materials

Fig. 7a and b shows the UV–vis spectra and efficiency of decolorization of the orange G solution with this electrochemical photocatalytic degradation process. Fig. 7a shows two absorption bands (ca. 255 and 330 nm) and a broad wave (465 and 490 nm) with a shoulder (400 nm) on the UV–vis spectra for the standard test solution. The intensity of these absorption bands gradually decreased with degradation time, showing that orange G can be decolorized and/or decomposed by electrochemical photocatalytic degradation. Note that the broad wave should be considered as two peaks and the decay rate in the absorption intensity for the peak at 465 nm is faster than that for the peak centered at 490 nm. Also note that in this degradation process, P25-TiO_2/SS was used as the working electrode with an applied electrode potential of 1.0 V (vs. SCE) under UV illumination, while pure oxygen gas was pumped around counter electrode at a flow rate of 50 mL min^{-1}. With a platinum sheet as the counter electrode was, the corresponding electrode potential was −0.29 V (vs. SCE) and after the 180-min degradation test 25.7% of the orange G had been decolored at 478 nm. However, when a graphite sheet was used as the counter electrode, the corresponding quasi-steady-state potential was shifted to −0.45 V

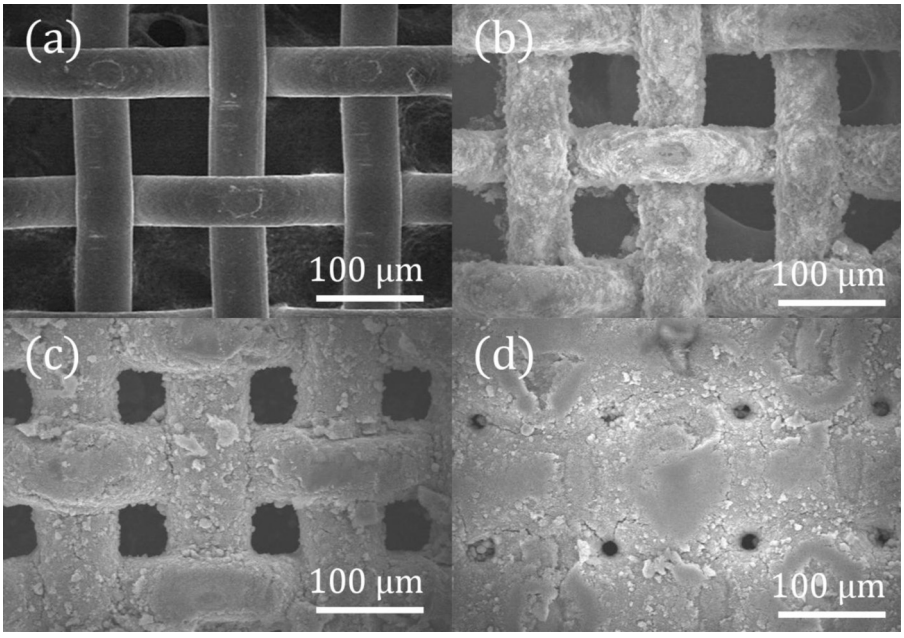

Fig. 5. SEM images of (a) a SS mesh and (b-d) P25-TiO_2/SS electrodes with (b) 1, (c) 3, and (d) 5 min of the EPD time. These P25-TiO_2/SS electrodes were annealed at 350 °C for 1 h.

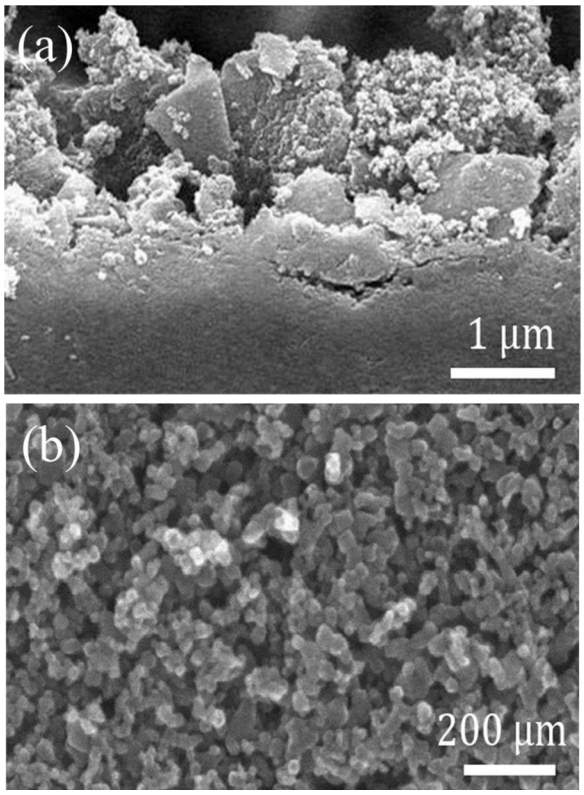

Fig. 6. (a) Surface morphological SEM images and (b) the cross-sectional of a P25-TiO_2/SS electrode with 1 min of the EDP time. The P25-TiO_2/SS electrode was annealed at 350 °C for 1 h

(vs. SCE), and the de-colorization rate increased to 36.7% when the same degradation test was carried out. Clearly, in comparison with Pt, graphite is a more suitable catalyst for the oxygen reduction reaction (ORR) with two-electron transfer to generate H_2O_2 [34], leading to a higher percentage de-colorization. This result also demonstrates our hypothesis that the electrochemical photocatalytic degradation process developed in this study must involve homogeneous catalytic degradation resulting from the generation of H_2O_2.

In order to substantiate this hypothesis further, linear sweep voltammetry (LSV) was used to characterize the electrocatalytic activity of Pt and graphite for H_2O_2 generation. LSV measurement was conducted at 5 mV s^{-1} in an acidic (pH 3.0), oxygen-saturated solution containing 10 mM Na_2SO_4. Typical results are shown in Fig. 8. From curve 1, reduction currents on the Pt electrode are visible at potentials negative to 0.2 V and the presence of a small reduction wave at ca. −0.3 V is attributable to the diffusion effect of dissolved oxygen molecules. The obvious increase in the cathodic current density at potentials negative to −0.95 V is a result of the hydrogen evolution reaction (HER), since Pt is a well-known electrocatalyst for this reaction, and extensive bubbles are visible. Curve 2, by contrast, shows a low background current density from 0 to −0.35 V and is considered as a double-layer charging current of graphite; the ORR starts at ca. −0.35 V when the graphite sheet is used. Further, a plateau corresponding to the limiting current density of the ORR on graphite was found from −0.7 to ca. −1.6 V, and the HER occurs at −1.6 V, leading to the sharp increase in cathode current density in this potential range. Clearly, graphite is a poor electrocatalyst for the HER, which provides a wider potential window for the ORR to generate H_2O_2. Moreover, the quasi-steady-state potential of the ORR on the graphite cathode was equal to −0.45 V (see Section 3 for Fig. 7), indicating the effective generation of H_2O_2. The more effective generation of H_2O_2 on the graphite

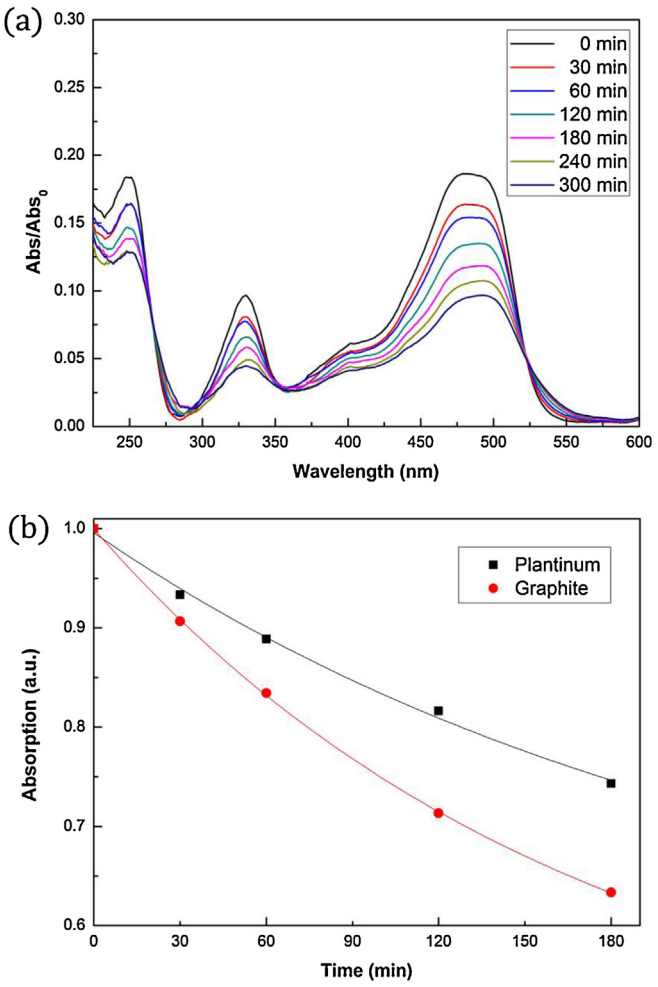

Fig. 7. (a) The dependence and (b) the UV–vis absorption spectra of absorption intensity of orange G against the degradation time in an oxygen-saturated solution containing 10 mM Na_2SO_4 and 64.0 mg L^{-1} orange G with pH 3. The electrochemical photocatalytic degradation used a P25-TiO_2/SS mesh electrode as the photo-anode under UV light irradiation and a graphite (or Pt) sheet as the cathode.

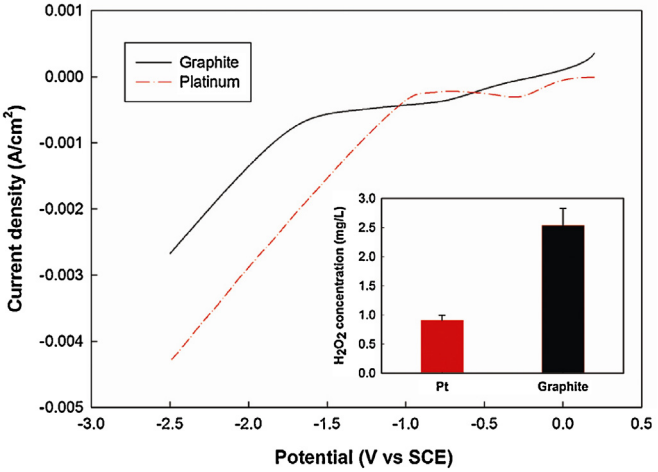

Fig. 8. Linear sweep voltammograms of (1) Pt and (2) graphite cathodes in an oxygen-saturated solution containing 10 mM Na_2SO_4 and 64.0 mg L^{-1} orange G with pH 3. Inset shows the corresponding concentration of H_2O_2 after the photoelectrochemical process for 180 min.

electrode in comparison with the Pt sheet is strongly supported by the results shown in the inset of Fig. 8, where a much higher H_2O_2 concentration in the test media (without adding orange G) was obtained when the electrochemical photocatalytic degradation reactor was operated for 180 min under the same conditions as shown in Fig. 7. In previous studies [34,35], the electron transfer number for the ORR on Pt was found to be very close to 4, which can be simply expressed as follows:

$$O_2 + 4H^+ + 4e \rightarrow 2H_2O \quad (4)$$

while the electrocatalytic generation of H_2O_2 through the 2-electron ORR mechanism can be described as [36]:

$$O_2 + 2H^+ + 2e \rightarrow H_2O_2 \quad (5)$$

A higher de-colorization percentage could thus be obtained when graphite is used as the catalytic cathode for the H_2O_2 generation.

3.3. Comparisons of different degradation modes

Fig. 9a shows the typical cyclic voltammograms of a bare SS mesh and a P25-TiO_2/SS electrode measured at 10 mV s^{-1} in the blank testing solution (i.e., a pH 3.0 oxygen-saturated solution containing 10 mM Na_2SO_4). On the positive sweep of curve 1, anodic current is found when the potentials are 0.2 V. The SS substrate is stable at potentials less than ca. 0.6 V in this weak acidic media without corrosive agents, since only background current is visible in this region. However, the current density starts to increase when the electrode potential is greater than 0.6 V, indicating the significant oxidation of SS, which may lead to the release of ferrous ions into the solutions. This irreversible oxidation is clearly visible on both positive and negative sweeps in the same potential region. The larger background current densities on the negative sweep from 0.6 to 0.2 V might be due to the reduction of hydroxides formed at potentials positive to 0.6 V, since oxygen reduction should occur at potentials less than 0.2 V from the LSV result measured on a Pt electrode (see Fig. 8). On curve 2, the background currents of the P25-TiO_2/SS electrode in the whole potential region are much smaller than that of a bare SS substrate. The minor oxidation currents at potentials greater than 0.8 V indicate that the P25-TiO_2 deposit significantly increases the anticorrosion ability of SS, although the SS mesh with a porous P25-TiO_2 coating corrodes slightly in the weak acid medium at highly positive potentials. The TiO_2/SS electrodes showed approximately the same activity for the electrochemical photocatalytic degradation of orange G after repeated electrochemical photocatalytic degradation test. This result suggests the stability of the TiO_2/SS electrodes in the electrochemical photocatalytic degradation test.

In order to confirm the photosensitive ability of the P25-TiO_2/SS electrode, this electrode was examined by cyclic voltammetry under both dark and UV illumination conditions (see Fig. 9b). A comparison of the positive sweeps on curves 1 and 2 shows that higher anodic current densities were obtained at potentials greater than −0.1 V when the P25-TiO_2/SS electrode was irradiated with UV light. Further, the corresponding negative sweeps show that the anodic photocurrent contribution from the photo-excited electrons reduced the cathodic background current density at potentials positive to 0 V. These results tell us that P25-TiO_2 is an n-type semiconductor and that P25-TiO_2 is sensitive to UV irradiation, and generates photo-excited electrons which can be driven by a positive electric field from the P25-TiO_2/SS photo-anode to the graphite cathode for generating H_2O_2 via the two-electron-transfer ORR mechanisms. In addition, the applied electrode potential, 1.0 V, on P25-TiO_2/SS can increase the ORR current density from 26.4 to 29.8 μA cm^{-2} (i.e. by ca. 13%). The 13% increase is contributed by the photo-excited electrons generated on the P25-TiO_2/SS photo-anode.

Fig. 10 shows the relative contributions of the electrochemical, photocatalytic, and electrochemical photocatalytic the carbon

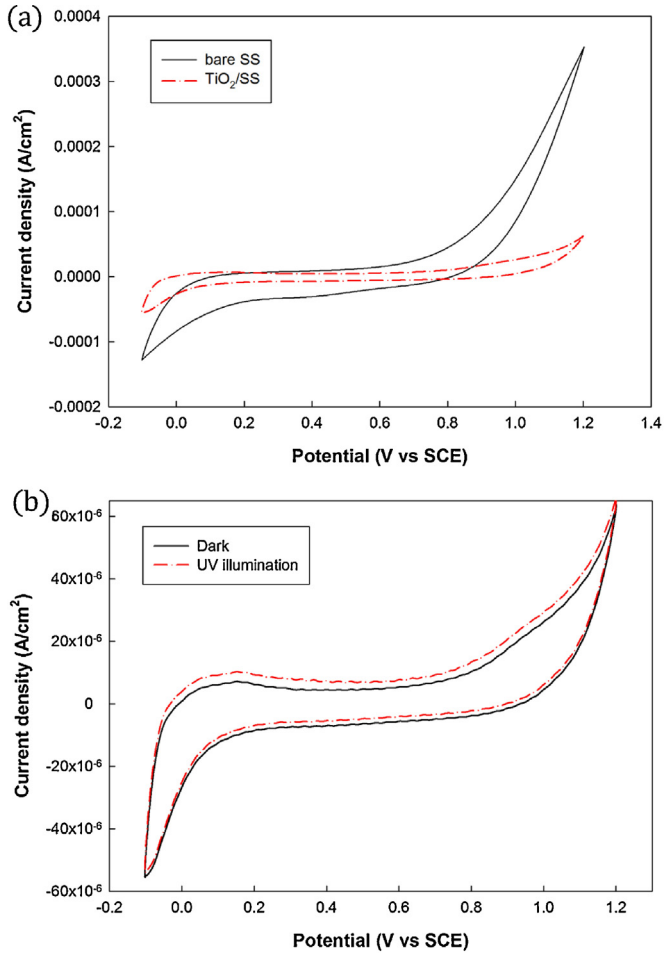

Fig. 9. Cyclic voltammograms of (a) a bare SS mesh and a P25-TiO_2/SS electrode in dark and (b) a P25-TiO_2/SS electrode in dark and under UV light irradiation in an oxygen-saturated solution containing 10 mM Na_2SO_4 and 64.0 mg L^{-1} orange G with pH 3.

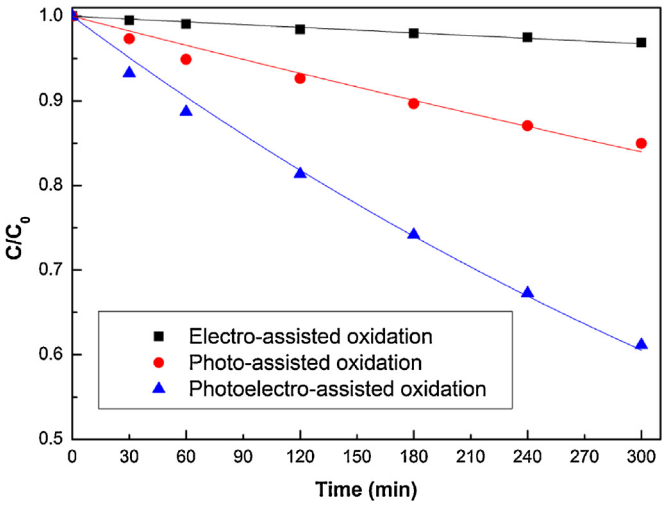

Fig. 10. The DOC removal profiles in an oxygen-saturated solution containing 10 mM Na_2SO_4 and 64.0 mg L^{-1} orange G with pH 3 under (1) electrochemical, (2) photocatalytic, and (3) electrochemical photocatalytic degradation modes.

removal by degradation in the standard test solution. In the pure electrochemical process with 1.0 V applied to the P25-TiO_2/SS anode coupled with a graphite cathode, the DOC value decreased by only 3.1% (from 64.0 to 62.0 mg L^{-1}) after potentiostatic electrolysis for 300 min. Since the electrode potential is not high enough to force an oxygen-transfer reaction [37], the removal of carbon can mainly be attributed to an indirect catalytic oxidation process (i.e. the electro-Fenton process). In this case, ferrous ions might be generated from the SS substrate even though it had been coated with a thin, macroporous P25-TiO_2 layer. These metallic ions would penetrate the porous P25-TiO_2 layer and flow into the orange G solution, while H_2O_2 could be produced at the graphite cathode. Thus, an electro-Fenton reaction occurred in the test solution, reducing the DOC value. Here the concentration of ferrous ions is lower than 0.33 mg L^{-1} after a 300-min electrolytic treatment. Fig. 10 also shows the result of a pure photocatalytic oxidation process where the P25-TiO_2/SS electrode was irradiated with UV light for 300 min. The DOC value was significantly decreased from 64.0 to 54.2 mg L^{-1} (about 15%) through a photocatalytic degradation mechanism, although the photo-excited electrons may flow to the graphite cathode to drive the two-electron-transfer ORR for producing H_2O_2. However, the SS substrate must be protected by the photo-excited electrons as demonstrated in previous work/experiments [38]. Hence, an electro-Fenton reaction did not occur in this pure photocatalytic oxidation process.

For the electrochemical photocatalytic degradation system, the electrode potential of the TiO_2/SS photo-anode was fixed at 1.0 V, and was irradiated with UV-light. The DOC value decreased by 38.8% after a 300-min degradation treatment. The concentration of ferrous ions in the test solution was very close to that in the pure electrochemical process, at 0.38 mg L^{-1}. However, the orange G mineralization rate in this degradation process (DOC reduction = 38.8%) was much higher than the sum of the pure electrochemical oxidation (3.1%) and pure photocatalytic degradation (15%) processes, demonstrating a synergistic effect on the mineralization of orange G. This phenomenon was attributed to a combination of (1) effective reduction of the photo-excited electron/hole pair self-recombination (favorable for direct oxidation) and (2) the significant contribution of the electro-Fenton reaction induced by the electric field (indirect oxidation). Accordingly, the above integration of direct and indirect oxidation processes can be termed as photoelectrocatalysis (PEC).

3.4. Effects of pH

In general, the pH value of the test solution is important in advanced oxidation processes such as photocatalytic degradation [39] and Fenton reactions [40]. In this section, the influence of the test solution pH on orange G mineralization in the electrochemical photocatalytic degradation was investigated by varying the pH value from 3 to 9, and the results for pHs of 3, 6, and 9 are shown in Fig. 11. The other operating conditions followed those applied for the electrochemical photocatalytic degradation system, shown in Fig. 10. Note that at pH 9, the pseudo-steady-state current on the photo-anode was about 78 μA, while the DOC removal was only 1.8% after the 180-min degradation test. This result shows the very poor efficiency of electrochemical photocatalytic degradation in weak basic media, attributable to the ineffective Fenton regent in this medium [40]. When pH was set at 6.0, the pseudo-steady-state current on the photo-anode increased to 234 μA, implying a higher photocurrent for H_2O_2 generation. The DOC removal in this medium thus increased from 1.8 to 11.8% after the same degradation treatment. Moreover, with pH 3.0, the pseudo-steady-state current on the photo-anode further increased to 310 μA. The DOC removal in this case reached 25.8% after a 180-min treatment. The above exponential increase in the DOC removal by increasing the pseudo-steady-state current on the photo-anode implies that the electro-Fenton oxidation may dominate the DOC removal in this process.

It is well known that the photocatalytic degradation of organic pollutants by means of TiO_2 generally follows Langmuir–Hinshelwood (L–H) kinetics. Hence, a kinetic model of the first-order reaction is usually used to describe the photocatalytic degradation and the PEC reaction [41]. Based on this model, the experimental data shown in Fig. 11a were fitted by Eq. (6):

$$\frac{C}{C_0} = \exp(-kt) \tag{6}$$

where the pseudo-first-order kinetic constant, k, obtained from data fitting could be used to evaluate the total oxidation rate. The experimental results indicate that the k values obtained from the test solutions with pH 3, 6, and 9 are equal to 1.690×10^{-2}, 7.31×10^{-3}, and 1.07×10^{-3} min^{-1}. Clearly, the highest rate of DOC removal was obtained from the test solution with pH 3.

The exact reasons why the pseudo-steady-state currents on the photo-anode increased with decreasing the pH value in the test solution are unclear. This effect has been confirmed to change the concentration of electrogenerated H_2O_2 (see Fig. 11b), leading to different degrees of orange G mineralization. From the literature [42], electrogenerated H_2O_2 has been found to be more stable in more acidic media. Furthermore, the formation of HO_2^- anions

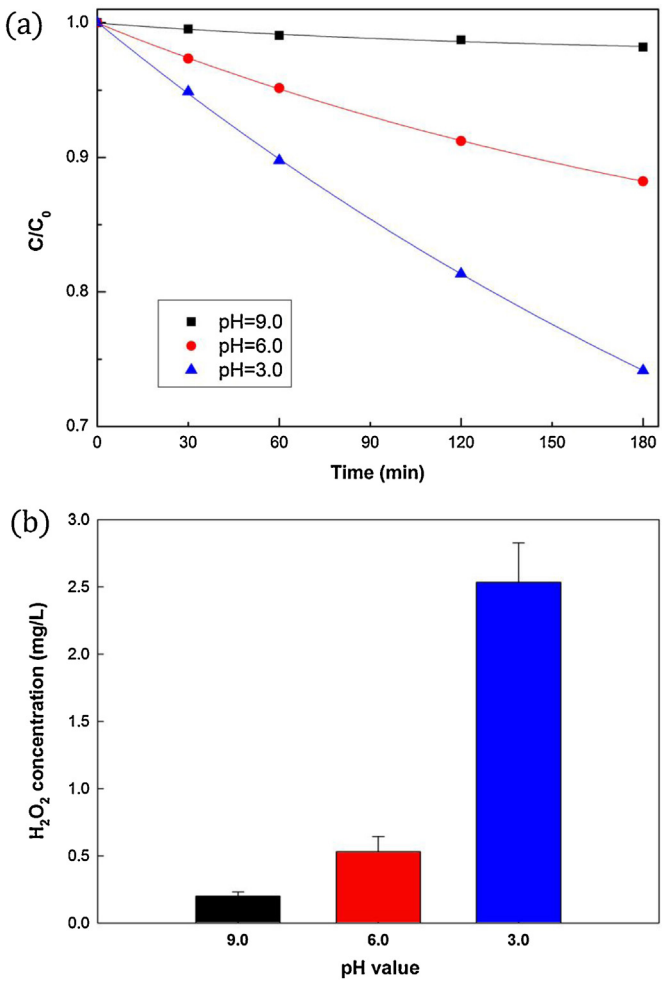

Fig. 11. (a) The DOC removal profiles and (b) the corresponding concentration of H_2O_2 produced in an oxygen-saturated solution containing 10 mM Na_2SO_4 and 64.0 mg L^{-1} orange G under the electrochemical photocatalytic degradation mode with solution pHs of (1) 3, (2) 6, and (3) 9 for 180 min.

in basic electrolyte solution would favor the disproportionation of H_2O_2, which can be expressed as [43]:

$$H_2O_2 + HO_2^- \rightarrow H_2O + O_2 + OH^- \quad (7)$$

Moreover, the pseudo-steady-state current on the photo-anode also decreased with increasing pH of the test solution, and the concentrations of electrogenerated H_2O_2 after an electrochemical photocatalytic test (without orange G) for 180 min were 3.10, 0.69, and 0.197 mg L^{-1} at pH 3, 6, and 9, respectively. Again, the results support the statement that the DOC removal rate is dominated by electro-Fenton indirect oxidation, although a synergistic effect between the electrochemical and photocatalytic degradation processes does exist.

3.5. Effects of electrode potentials on the anode and cathode

To extend this idea, a further increase in H_2O_2 and Fe^{2+} concentrations in the test solution should further be able to increase the DOC removal by means of this electrochemical photocatalytic degradation process. As described above under the electrochemical photocatalytic degradation with a biased electrode potential of 1.0 V on the TiO_2/SS electrode, the corresponding potential on the graphite cathode was equal to −0.4 V, and the concentration of electrogenerated H_2O_2 was 3.1 mg L^{-1} after the 300-min treatment. From curve 2 in Fig. 8, it can bes seem that the current density obtained at −0.4 V for the graphite electrode is not in the diffusion control region for generating H_2O_2. As a result, the electrode potential of the graphite cathode was fixed at −1.0 V (vs. SCE) to increase the concentration of electrogenerated hydrogen peroxide. Note that when the graphite sheet was biased at −1.0 V (vs. SCE), the corresponding electrode potential on the TiO_2/SS electrode was positively shifted to 2.0 V (vs. SCE). These results indicate that under electrochemical photocatalytic degradation, a further increase in the H_2O_2 and Fe^{2+} concentrations in the test solution would be achieved by applying a constant potential of −1.0 V on the graphite cathode. The above phenomenon has been demonstrated in Fig. 12a where the concentrations of both ferrous ions and hydrogen peroxide were simultaneously increased to from 0.38 and 3.1 mg L^{-1} to 4.5 and 13.0 mg L^{-1}, respectively. Furthermore, the biased electrode potential at 2.0 V may result in the direct oxidation of organics through the oxygen-transfer reaction path [37], which is also favorable for the DOC removal.

The proposal that the DOC removal rate can be further enhanced by increasing both ferrous ion and hydrogen peroxide concentrations in order to boost the electro-Fenton process in the electrochemical photocatalytic degradation process is shown in Fig. 12b. Obviously, as the graphite sheet was biased at −1.0 V, the DOC removal percentage reached 63.9%. In comparison with the same process with the P25-TiO_2/SS electrode biased at 1.0 V, this oxidation process performance better, in either de-colorization or mineralization of orange G, than when the process was operated under the diffusion control of the electrochemical generation of H_2O_2.

3.6. Influences of orange G

The question has been raised whether organic dyes may act as photo-sensitizer that increase the organic degradation rate in this combined electrochemical and photocatalytic system [44]. In response to this, a different organic compound, bisphenol A (BPA) which is not a dye and is hazardous to bio-organisms, was tested. Fig. 13 shows the relative contribution of the electrochemical, photocatalytic, and electrochemical photo-catalytic degradation process in the removal of carbon removal from the test solution containing 10 mg L^{-1} BPA. A result similar to that of Fig. 10 was found. After a 210-min treatment, the order of the processes by

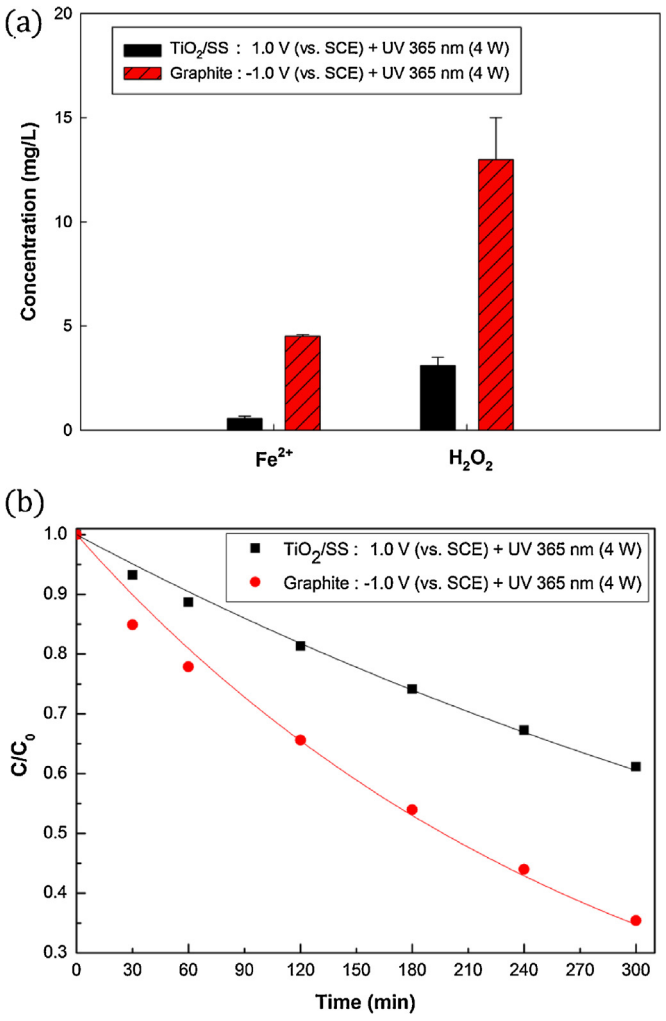

Fig. 12. (a) The corresponding DOC removal profile and (b) The concentrations of Fe^{2+} and H_2O_2 produced in an oxygen-saturated solution containing 10 mM Na_2SO_4 and 64.0 mg L^{-1} orange G with pH 3 (1) as the P25-TiO_2/SS electrode was biased at 1.0 V (vs. SCE) and (2) as the graphite cathode was biased at −1.0 V (vs. SCE) under the electrochemical photocatalytic degradation mode for 300 min.

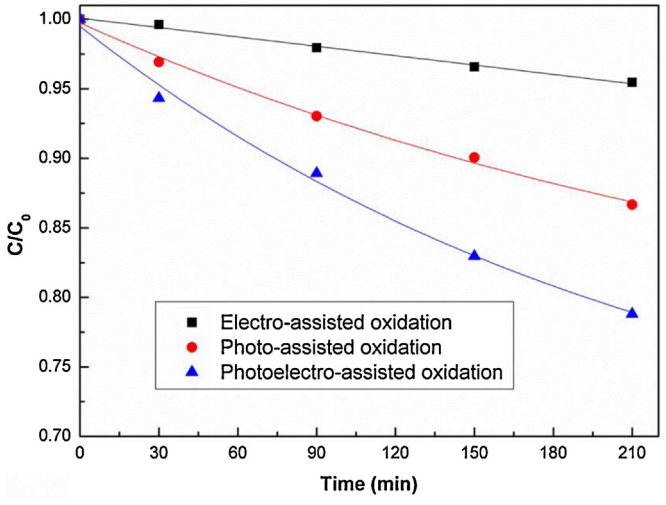

Fig. 13. The DOC removal profiles in an oxygen-saturated solution containing 10 mM Na_2SO_4 and 10 mg L^{-1} BPA with pH 3 under (1) electrochemical, (2) photocatalytic, and (3) electrochemical photocatalytic degradation modes.

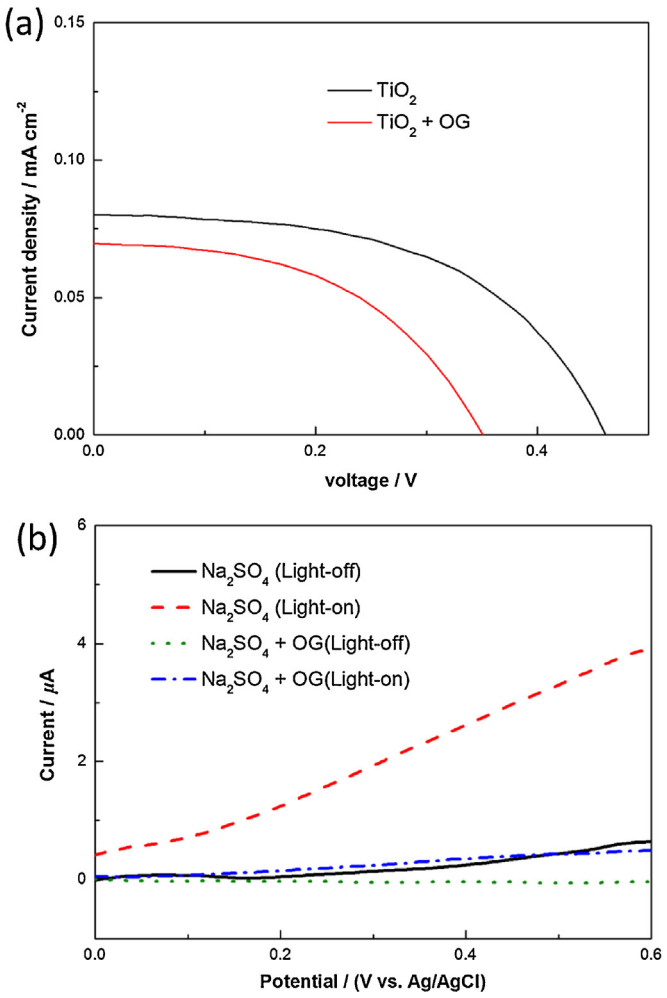

Fig. 14. (a) The photocurrent-voltage curves of a DSSC employing (1) orange G as the dye on the TiO_2 photo-anode and (2) a bare TiO_2 photo-anode. (b) LSV curves measured at 5 mV s^{-1} in (1,2) 10 mM Na_2SO_4 and (3,4) 10 mM Na_2SO_4 + 64.0 mg L^{-1} orange G with pH 3 in (1,3) dark and (2,4) under UV-light irradiation.

which DOC is removed is: electrochemical photocatalytic process (DOC reduction = 21.2%) > photocatalytic degradation only (DOC reduction = 13.3%) > electrochemical oxidation only (DOC reduction = 4.5%). Further, the BPA mineralization rate in the combined degradation process was significantly higher than the sum of the pure electrochemical oxidation plus photocatalytic degradation, showing a synergistic effect by combing the electrochemical and photocatalytic oxidation processes on the mineralization of organics. Based on the results and discussion for Figs. 10 and 13, the integration of direct and indirect oxidation processes can be termed photoelectrocatalysis (PEC), which produces a synergistic DOC removal of orange G and BPA. It also confirms that orange G is not a photo-sensitizer that enhances the organic degradation in this synergistic oxidation process.

To further clarify the possible influences of orange G on PEC efficiency, the photo-electrochemical behavior of orange G was evaluated by photovoltaic and photo-electrochemical tests with results given in Fig. 14. Fig. 14a shows the current–voltage curves of a dye-sensitized solar cell (DSSC) without and with orange G as the dye. Clearly, using orange G in a typical DSSC reduced the open-circuit voltage (V_{OC}) and the short-circuit current (J_{SC}) of the cell using TiO_2 photo-anode. The results also show that the photo-excited electrons on the adsorbed orange G cannot be effectively injected into TiO_2, probably because of the incompatible conduction bands between orange G and TiO_2 (e.g. the potential of the conduction band on orange G is lower than that on TiO_2). Moreover, the adsorbed orange G shields TiO_2 from UV radiation and reduces the photocurrent generated from TiO_2. As a result, the photovoltaic performances of a DSSC with the orange G dye are much worse than those of a DSSC without any dye.

The above is supported by the LSV curves shown in Fig. 14b. Note the low background current on curve 1, indicating the typical double-layer responses of TiO_2 in the aqueous Na_2SO_4 solution, since TiO_2 is inert in the test electrolyte. On curve 2, a sharp increase in the background current from 0.02 to 0.5 μA at the initial applied potential indicates the contribution of photocurrent from TiO_2 excited by the UV-light irradiation. This photocurrent is gradually increased by the positive shift in the electrode potential, since the positively-biased potential favors the charge separation of photo-excited electrons and holes [19]. On curve 3, the background current of TiO_2 in the Na_2SO_4 + orange G solution is lower than that of TiO_2 in the blank electrolyte (see curve 1). This decrease in the double-layer current can reasonably be attributed to the adsorption of orange G on TiO_2 surface, which reduces the double-layer capacitance of TiO_2. Thus the adsorbed orange G might act as a photo-sensitizer if the photo-excited electrons on the adsorbed orange G can be effectively injected into TiO_2. From curve 4, however, it can be seen that the photocurrent on TiO_2 is obviously decreased by the adsorption of orange G, showing that the photo-excited electrons on the adsorbed orange G cannot be injected into TiO_2. Again, the adsorbed orange G shields TiO_2 from the UV-light irradiation and reduces the photocurrent generated from TiO_2. Based on all these above results and discussion in this section, orange G cannot act as a photo-sensitizer to promote the efficiency of photoelectrocatalysis for organic degradation.

4. Conclusions

In this study, P25-TiO_2 powder was successfully deposited onto the surface of SS mesh via an electrophoretic deposition method. The physicochemical characteristics of P25-TiO_2 were not significantly changed by the EPD process and annealing at 350 °C for 1 h. A synergistic effect on the degradation of orange G was obtained when an electro-Fenton and a photocatalytic oxidation process occurred simultaneously in the photo-electrochemical reactor. Under UV-light radiation, ferrous ions dissolved from the P25-TiO_2/SS photo-anode and H_2O_2 generated from the graphite cathode resulted in an electro-Fenton (indirect oxidation) process, and the photo-excited holes drove the direct photocatalytic oxidation process, especially when the graphite cathode was biased at −1.0 V (vs. SCE). This newly developed synergistic oxidation method could be considered as an advanced wastewater treatment process for pollutants which could not be effectively removed or decomposed by common AOPs.

Acknowledgment

The authors dedicate this manuscript to Prof. Jill R Pan, who sank into a coma after suffering a brain hemorrhage when she finished this revised paper on February 22 in 2013. Unfortunately after one week, she has passed away. Without her input this work would not have been possible. The financial support of this work by the Technology Development Program, Ministry of Economic Affairs of the Republic of China is gratefully acknowledged.

References

[1] M. Banat, P. Nigam, D. Singh, R. Marchant, Bioresource Technology 58 (1996) 217–227.
[2] H.A. Moreno-Casillas, D.L. Cocke, J.A.G. Gomesa, P. Morkovsky, J.R. Parga, E. Peterson, Separation and Purification Technology 56 (2007) 204–211.

[3] M.A. Oturan, Journal of Applied Electrochemistry 30 (2000) 475–482.
[4] N. Mohan, N. Balasubramanian, C.A. Basha, Journal of Hazardous Materials 147 (2007) 644–651.
[5] H. Choi, E. Stathatos, D.D. Dionysiou, Applied Catalysis B: Environmental 63 (2006) 20–27.
[6] J.H. Sun, S.H. Shia, Y.F. Lee, S.P. Sun, Chemical Engineering Journal 155 (2009) 680–683.
[7] D. Hermosillaa, M. Cortijob, C.P. Huang, Chemical Engineering Journal 155 (2009) 637–646.
[8] M.S. Lucas, J.A. Peres, Dyes and Pigments 71 (2006) 236–244.
[9] T.-T. Tsai, J. Sah, C.-M. Kao, Journal of Hydrology 380 (2010) 4–13.
[10] M.A. Oturan, J-J. Aaron, N. Oturan, J. Pinson, Pesticide Science 55 (1999) 558–562.
[11] P.C. Foller, R.T. Bombard, Journal of Applied Electrochemistry 25 (1995) 613–627.
[12] S. Chou, Y.-H. Huang, S.-N. Lee, G.-H. Huang, C. Huang, Water Research 33 (1999) 751–759.
[13] J.M. Peralta-Hernandez, Y. Meas-Vong, F.J. Rodriguez, T.W. Chapman, M.I. Maldonado, L.A. Godinez, Water Research 40 (2006) 1754–1762.
[14] A. Di Paola, G. Cufalo, M. Addamo, M. Bellardita, R. Campostrini, M. Ischia, R. Ceccato, L. Palmisanoa, Colloids and Surfaces A: Physicochemical and Engineering Aspects 317 (2008) 366–376.
[15] Y.B. Xie, X.Z. Li, Matrials Chemistry and Physics 95 (2006) 39–50.
[16] C. Tang, V. Chen, Water Research 38 (2004) 2775–2781.
[17] Y.B. Xie, X. Li, Materials Chemistry and Physics 95 (2006) 39–50.
[18] H. Park, K.Y. Kim, W. Choi, The Journal of Physical Chemistry B 106 (2002) 4775–4781.
[19] P.A. Carneiro, M.E. Osugi, J.J. Sene, M.A. Anderson, M.V.B. Zanoni, Electrochimica Acta 49 (2004) 3807–3820.
[20] I.M. Arabatzis, S. Antonaraki, T. Stergiopoulos, A. Hiskia, E. Papaconstantinou, M.C. Bernard, P. Falaras, Journal of Photochemistry and Photobiology A: Chemistry 149 (2002) 237–245.
[21] L. Bamoulid, M.T. Maurette, D. De Caro, A. Guenbour, A. Ben Bachir, L. Aries, S. El Hajjaji, F. Benoît-Marquié, F. Ansart, Surface and Coatings Technology 202 (2008) 5020–5026.
[22] T. Ma, T. Kida, M. Akiyama, K. Inoue, S. Tsunematsu, K. Yao, H. Noma, E. Abe, Electrochemistry Communications 5 (2003) 369–372.
[23] S. Ito, P. Chen, P. Comte, M.K. Nazeeruddin, P. Liska, P. Péchy, M. Grätzel, Progress in Photovoltaics: Research and Applications 15 (2007) 603–612.
[24] B.C. Kang, S.B. Lee, J.H. Boo, Surface and Coatings Technology 131 (2000) 88–92.
[25] S. Klosek, D. Raftery, The Journal of Physical Chemistry B 105 (2001) 2815–2819.
[26] Y.B. Xie, X.Z. Li, Journal of Hazardous Materials 138 (2006) 526–533.
[27] K. Wessels, M. Maekawa, J. Rathousky, T. Oekermann, Thin Solid Films 515 (2007) 6497–6500.
[28] C.C. Huang, H.C. Hsu, C.C. Hu, K.H. Chang, Y.F. Lee, Electrochimica Acta 55 (2010) 7028–7035.
[29] W. Tan, X. Yin, X. Zhou, J. Zhang, X. Xiao, Y. Lin, Electrochimica Acta 54 (2009) 4467–4472.
[30] T. Sridhar, N. Eliaz, U. Kamachi Mudali, B. Raj, Corrosion Reviews 20 (2002) 255–294.
[31] Z. Zhang, Y. Huang, Z. Jiang, Journal of the American Ceramic Society 77 (1994) 1946–1949.
[32] N. Barati, M.A. Faghihi Sani, H. Ghasemi, Z. Sadeghian, S.M.M. Mirhoseini, Applied Surface Science 255 (2007) 8328–8333.
[33] R.R. Bacsa, J. Kiwi, Applied Catalysis B: Environmental 16 (1998) 19–29.
[34] Y.H. Lee, F. Li, K.H. Chang, C.C. Hu, T. Ohsaka, Applied Catalysis B: Environmental 123 (2012) 208–214.
[35] R.H. Petrucci, W.S. Harwood, F.G. Herring, General Chemistry (Prentice Hall) 8th ed (2002) 460–1150.
[36] P.C. Foller, R.T. Bombard, Journal of Applied Electochemistry 25 (1995) 613.
[37] C. Zhou, Q. Yu, L. Lei, Dyes and Pigments 77 (2008) 129–136.
[38] L. Bamoulid, M.T. Maurette, D.D. Caro, A. Gouenbur, A.B. Bachir, L. Aries, S.E. Hajjaji, F. Benoît- arquié, F. Ansart, Surface and Coatings Technology 202 (2008) 5020–5026.
[39] S. Kaur, V. Singh, Journal of Hazardous Materials 141 (2007) 230–236.
[40] E. brillas, I. Sires, M.A. Oturan, Chemical Reviews 109 (2009) 6570–6631.
[41] K.V. Kumar, K. Porkodi, F. Rocha, Catalysis Communications 9 (2008) 82–84.
[42] Z. Qiang, J.H. Chang, C.P. Huang, Water Research 36 (2002) 85–94.
[43] E. Abel, Monatshefte für Chemie/Chemical Monthly 83 (1952) 422–439.
[44] J.M. Herrmann, Applied Catalysis B: Environmental 99 (2010) 461–468.